Proceedings of CHT-17
ICHMT International Symposium on Advances in Computational Heat Transfer

May 28 – June 2, 2017, Napoli, Italy

CHT-17-189

CONVECTIVE FLOW OF A BINGHAM FLUID IN AN INTERNALLY-HEATED POROUS ENCLOSURE

D. Andrew S. Rees
Department of Mechanical Engineering, University of Bath,
Claverton Down, Bath BA2 7AY, United Kingdom.
Email: D.A.S.Rees@bath.ac.uk

ABSTRACT A rectangular porous cavity is saturated with a Bingham fluid and is subjected to a uniform internal heat generation while all the bounding surfaces are held at the same fixed temperature. When the porous medium is saturated by a Newtonian fluid then convection takes place at all nonzero values of the Darcy-Rayleigh number, Ra, and at moderate values of Ra, convection takes the form of two contra-rotating cells with flow down the cold sidewalls. However, when the enclosure is saturated by a Bingham fluid, then we find that no flow takes place when the Darcy-Rayleigh number is below a critical value because buoyancy forces are too weak to overcome the yield threshold.

Numerical solutions are obtained using a second order accurate finite difference methodology where convergence is accelerated using line-relaxation and the Full Approximation Scheme multigrid method. The presence of the yield surfaces, which mark the boundaries of stagnant regions, is modelled by means of a regularisation of the yield threshold.

It is found that the critical value of Ra above which convection arises depends linearly on the value of Rb, which may be described as a convective porous Bingham number. It is also found that, as Ra increases, the proportion of the cavity which is not stagnant also increases, but stagnant regions always exist and are found within the middle of the two circulations, near the corners of the cavity and on the horizontal boundaries near the middle of the cavity.

INTRODUCTION

The flow of Bingham fluids in porous media is a well-established topic with a variety of important industrial applications, particularly some in the oil industry. A Bingham fluid is characterized by having a yield stress, by which is meant that the fluid exhibits no rate of strain (equivalently no velocity gradient) unless the local stresses exceed a critical value called the yield stress. When such a fluid occupies a pipe and is subject to pressure gradient along that pipe, then no flow arises until the pressure gradient exceeds a critical value which is dependent on the yield stress of the fluid and the radius of the pipe. Thereafter the flow consists of two regions, an outer annular region which exhibits and a the central region which is a moving, but unyielded plug flow. In the context of porous media, of which this pipe flow is a simplfied model, there is also a critical pressure gradient (or, equivalently, buoyancy forces when the medium is subjected to heating) below which no flow takes place. At sufficiently large pressure gradients the rate of flow is a linear function of the pressure gradient. Near the threshold gradient the variation in the rate of flow depends strongly on the microstructure of the porous medium; see Nash and Rees (2017).

The present work is part of a project which is examining the effect of the presence of a yield threshold on convective flows of a Bingham fluid in a porous medium. Previous works include free convective boundary layer flows (Rees 2015, Rees and Bassom 2015, 2016), and natural convection within a differentially heated cavity (Rees 2016). When saturated by a Newtonian fluid, the resulting flow and its

successive bifurcations depend quite strongly on the aspect ratio of the cavity. When the cavity has an infinite aspect ratio the basic conducting state, which is realisable when the Darcy-Rayleigh number is sufficiently small, is independent of the horizontal coordinate, x. Gasser and Kazimi (1976) used a linearised stability theory to show that convection ensues once Ra exceeds a certain critical value; Nouri-Borujerdi et al. (2007) have given this value to be 471.3787. However, when the aspect ratio of the cavity, (defined here as the width relative to the height) is finite, but large, the basic state consists of two weak circulations in the end-zones with the maximum temperature being obtained just above the centre of the cavity. The transition to a steady cellular convective state is now smooth, and new cells appear near the middle of the upper surface of the cavity (Banu 2000). Eventually, the flow becomes unsteady (Banu et al. 1998) and Banu (2000) indicates that, for example, for a cavity of aspect ratio equal to 2, an unsteady state may be obtained when Ra is as low as 2200.

In this work we shall confine most of our attention to a cavity with aspect ratio 2 and to values of Ra which are at or below 1000. The general aims are (i) to determine how the critical value of Ra varies with the Rees-Bingham number, Rb, for this cavity, and (ii) to obtain an understanding of how the fluid begins to flow once the critical value of Ra is exceeded. Our chosen range of values of Ra is below that when one expect persistently unsteady convection when the porous medium is saturated by a Newtonian fluid, and therefore, given the resistance to flow which is afforded by the Bingham fluid, it is an *a priori* and perfectly reasonable expectation that flows will be steady. Some flows for other aspect ratios are also presented.

GOVERNING EQUATIONS

The simplest unidirectional Darcy-Bingham law was given by Pascal (1981) and in nondimensional form it may be written in the form,

$$w = \begin{cases} -\Big[1 - \dfrac{\mathrm{Rb}}{|p_z|}\Big] p_z & \text{when } |p_z| > \mathrm{Rb}, \\ 0 & \text{otherwise.} \end{cases} \tag{1}$$

When buoyancy forces (subject to the Boussinesq approximation) are present this becomes,

$$w = \begin{cases} -\Big[1 - \dfrac{\mathrm{Rb}}{|p_z - \mathrm{Ra}\,\theta|}\Big] \big(p_z - \mathrm{Ra}\,\theta\big) & \text{when } |p_z - \mathrm{Ra}\,\theta| > \mathrm{Rb}, \\ 0 & \text{otherwise,} \end{cases} \tag{2}$$

where the corresponding Newtonian forms are obtained when $\mathrm{Rb} = 0$. In these equations,

$$\mathrm{Ra} = \frac{\rho g \beta \Delta T K L}{\mu \alpha}, \qquad \text{and} \qquad \mathrm{Rb} = \frac{GKL}{\mu\alpha}, \tag{3}$$

are the Darcy-Rayleigh and Rees-Bingham numbers, respectively (see Rees 2016). In (3) most of the terms correspond to their usual definitions, but specifically α is the thermal diffusivity, K the permeability, L the height of the cavity and G the yield pressure gradient. We will also take z to be the vertical coordinate.

The simulation of the flow of Bingham fluids is complicated greatly by the need to determine where the yield surface is. In porous media this locus divides regions of flow from regions which are stagnant. Here we will employ a regularisation which is similar to that of Papanastasiou (1987) to soften the effect of the yield threshold. This allows the fluid to have an artifically high viscosity when the body forces are small and to display a smooth transition to Pascal's threhold law as the driving body force increases. Thus Eq. (1) may be replaced by,

$$w + \mathrm{Rb}\tanh(cw/\mathrm{Rb}) = -p_z + \mathrm{Ra}\,\theta, \tag{4}$$

where c is an adjustable parameter. The threshold model is recovered when $c \to \infty$ (see Rees 2016). When w is sufficiently small, the left hand side of Eq. (4) takes the form, $(1 + c)w$, and therefore the artificially high viscosity referred to above is $(1 + c)$ larger than the post-yield viscosity.

The analogous frame-invariant system which governs isotropic two-dimensional convection is,

$$\Big[1 + \mathrm{Rb}\,\frac{\tanh(cq)}{q}\Big]u = -p_x, \tag{5}$$

$$\Big[1 + \mathrm{Rb}\,\frac{\tanh(cq)}{q}\Big]w = -p_z + \mathrm{Ra}\,\theta, \tag{6}$$

where the speed, q, is given by,

$$q^2 = u^2 + w^2. \tag{7}$$

The streamfunction may be introduced in the usual way using $u = -\psi_z$ and $w = \psi_x$, and we obtain the following momentum equation,

$$\nabla^2\psi + \frac{\mathrm{Rb}\,\tanh(cq/\mathrm{Rb})}{q^3}\Big[\psi_z^2\psi_{xx} - 2\psi_x\psi_z\psi_{xz} + \psi_x^2\psi_{zz}\Big] + \frac{c\,\mathrm{sech}^2(cq/\mathrm{Rb})}{q^2}\Big[\psi_x^2\psi_{xx} + 2\psi_x\psi_z\psi_{xz} + \psi_z^2\psi_{zz}\Big] = \mathrm{Ra}\,\theta_x, \tag{8}$$

where $q^2 = \psi_x^2 + \psi_y^2$. Any potential for apparently singular behaviour of the coefficients when q is small is avoided by replacing the left hand side of Eq. (8) by a five-term Maclaurin series in q when $q < 10^{-3}$; this gives a seemless transition to Fortran double precision accuracy as q crosses the 10^{-3} threshold. Finally, the heat transport equation is given by,

$$\theta_t = \nabla^2\theta + \psi_z\theta_x - \psi_x\theta_z + 1. \tag{9}$$

We confine attention to a 2×1 cavity and to $\mathrm{Ra} \le 1000$ for the most part in this paper. The boundary conditions are that $\psi = \theta = 0$ on all four boundaries; this is equivalent to impermeable boundaries which are held at identical temperatures. In practice, and in the range of values of Ra which we are considering, the resulting flow displays right/left symmetry, therefore we shall consider only the left-hand half of the cavity, where the boundary conditions at the central vertical plane are $\psi = 0$ and $\partial\theta/\partial x = 0$.

Two numerical codes were written. Each one employed a standard second-order accurate finite difference discretisation on a uniform grid. The first code used a pseudo-transient method whereby an additional single time derivative of ψ was added to the right hand side of Eq. (8). A simple Euler time-stepping scheme was used to march the solutions toward a steady-state. Steady state was deemed to be when the maximum change in θ between neighbouring timesteps was less than 10^{-8} in magnitude for 100 successive timesteps. The second code employed line-relaxation Gauss-Seidel with Full Approximation Scheme multigrid acceleration to solve the steady state forms of Eqs. (8) and (9). The convergence criterion for this code was that the residual for the temperature field needed to be less than 10^{-6}.

As has been discussed in detail in Rees (2016), there is a trade-off between the requirements of solving the governing equations accurately on a fine grid and and the need to use as large a value of c as is possible in order to model the yield surface accurately. Rees (2016) demonstrated that, for each chosen grid, there is a optimum value of c which allows the most accurate modelling of the yield threshold whilst still providing a robust convergence to a solution. In almost all cases here we use a uniform grid with the meshwidth, $1/128$, in both directions and with $c = 50$. This value of c corresponds, in effect, to a fluid with a viscosity which is 51 times that of the equivalent Newtonian flow when body forces are sufficiently small.

All the solutions which we report were obtained using the steady-state code. However, the two codes gave precisely the same results when the convergence criteria were made stronger (specifically the time-stepping code, where convergence to the steady-state is slow), but the steady-state code was considerably faster and was therefore chosen. Regions which are deemed to be stagnant are defined in the same way as described in Rees (2016).

NUMERICAL SOLUTIONS

Streamlines and isotherms for Rb = 5 are presented in Fig. 1 for a selection of values of Ra. Here we were able to use $c = 100$ for regularisation — this is also true for all our displayed streamlines and isotherms. In all figures of this type we display the computational region which was used, which is the left hand half of the full cavity.

The value Ra = 220 lies just above that value which admits convection as Ra increases. Indeed, the temperature field is almost identical to what one would obtain when solving $\nabla^2\theta + 1 = 0$ in the same cavity and therefore we see large regions of stagnation. Convection is induced by the presence of a cold sidewall on the left with higher temperatures to the right. There is a relatively strong but narrow region of flow down the sidewall, which weakens and widens as it turns the corner, traverses the lower surface and eventually completes its circuit. At such a near-critical value of Ra where the flow is weak, the regularisation is at its most inaccurate. This is why some streamlines may be found within the shaded stagnation region.

As Ra increases, the stronger buoyancy forces drive a stronger circulation and moving fluid occupies an increasing proportion of the cavity. When Ra = 1000 the temperature field is has changed quite markedly compared with that for Ra = 220 and the position of the maximum temperature in the cavity is now well above the mid-plane. In addition, the regions of stagnation have now decreased markedly in size and comprise roughly 4% of the cavity.

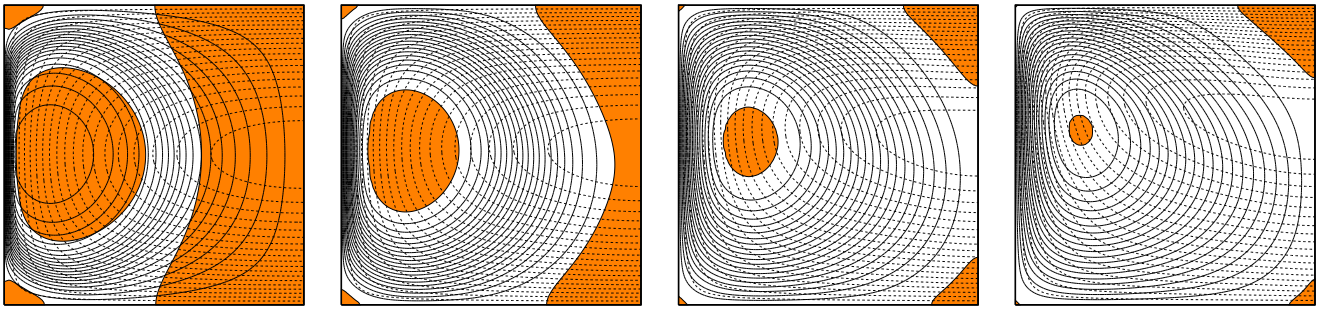

Figure 1. Streamlines (continuous) and isotherms (dashed) for $c = 100$ and Rb = 5. The stagnant regions are shaded in orange; these conventions apply to all figures of this type.

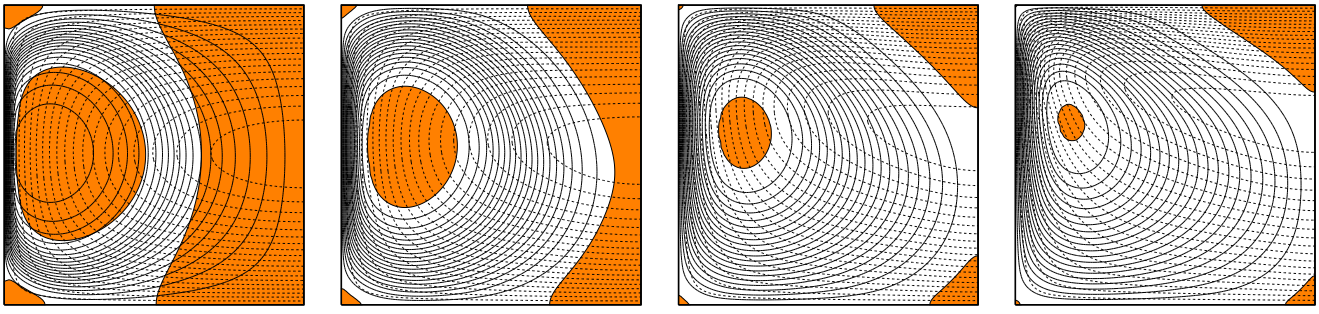

Figure 2. Streamlines (continuous) and isotherms (dashed) for $c = 100$ and Rb = 10.

Figure 2 shows streamlines, isotherms and stagnant regions for Rb = 10, and for values of Ra which are double the respective values used in Figure 1. It is quite clear that there is an exceptionally strong similarity between the respective frames in Figures 1 and 2, especially for the lower values of Ra. It is within this weak-flow regime that the response of the fluid is essentially linear because the nonlinear

terms in the heat transport equation are effectively neligible. This suggests that there will also be a linear relationship between Rb and the value of Ra above which fluid flows; we return to this idea later. However, at larger values of Ra, such as for Ra = 1000 when Rb = 5 in Figure 1 and Ra = 2000 when Rb = 10 in Figure 2, the magnitude of the excess of Ra over its critical value in the latter case is double that of the former, and therefore the flow is stronger in the latter case. Quantitative confirmation of these comments is provided in Table 1, below.

Table 1. Values of the maximum values of ψ and θ for chosen values of Ra and Rb. Also shown is ϕ, which is the fraction of the cavity in which the fluid is moving.

Rb	Ra	$\lvert\psi\rvert_{\max}$	$\theta_{\max}$	ϕ
5	220	0.0664	0.1139	0.380
5	300	0.364	0.1135	0.714
5	500	1.404	0.1090	0.917
5	1000	3.463	0.0944	0.959
10	440	0.133	0.1138	0.379
10	600	0.714	0.1125	0.709
10	1000	2.384	0.1020	0.890
10	2000	5.060	0.0831	0.932

The above Figures have summarised the general behaviour of the flow and temperature fields for a 2×1 cavity while within the regime where the flow is steady, and therefore no further Figures of this type need to be presented. However, a comprehensive summary of these flows is given in Figures 3 and 4 which show how $|\psi|_{\max}$ and $\theta_{\max}$ vary with Ra for integer values of Rb in the range 0 to 10. The numerical solutions were obtained at increments of 10 in the Darcy-Rayleigh number and the regularisation constant was set at $c = 50$, a value which presented no convergence difficulties.

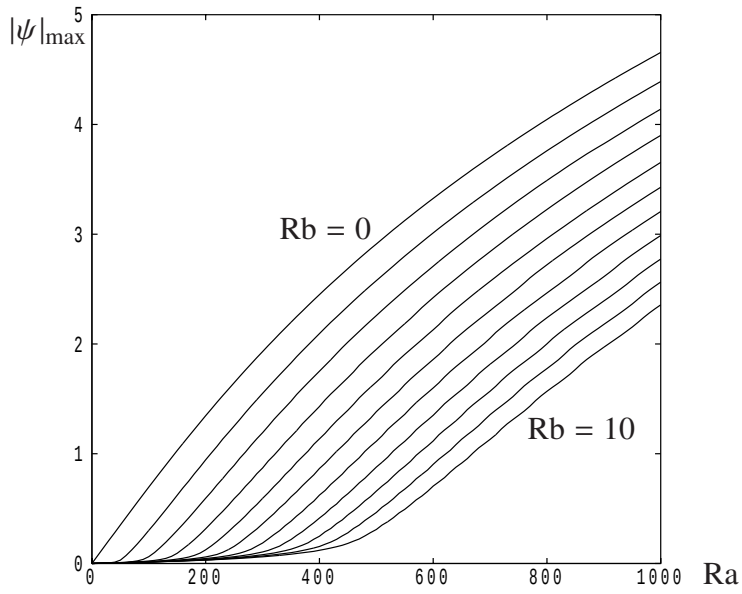

Figure 3. Variation with Ra of $|\psi|_{\max}$ for Rb taking integer values between 0 and 10.

The strength of the flow, as measured by $|\psi|_{\max}$, increases as Ra increases due to the increasing strength of buoyancy forces, but it decreases as Rb increases because the yield threshold of the Bingham

fluid becomes stronger. Indeed, the overall strength of the flow at Ra = 1000 at Rb = 10 is roughly half that for a Newtonian fluid, for which Rb = 0. The effect of the regularised form of Pascal's threshold model may be seen when $|\psi|_{\max}$ is small, i.e. when Ra is below its critical value for flow. Each curve joins an envelope which has a slope that is roughly 1/51 (i.e. $1/(c+1)$) that of the Rb = 0 curve at Ra = 0. For example, when Ra = 10 then $|\psi|_{\max} = 0.07052$ when Rb = 0, and $|\psi|_{\max} = 0.00138$ for all the Rb $\neq$ 0 curves.

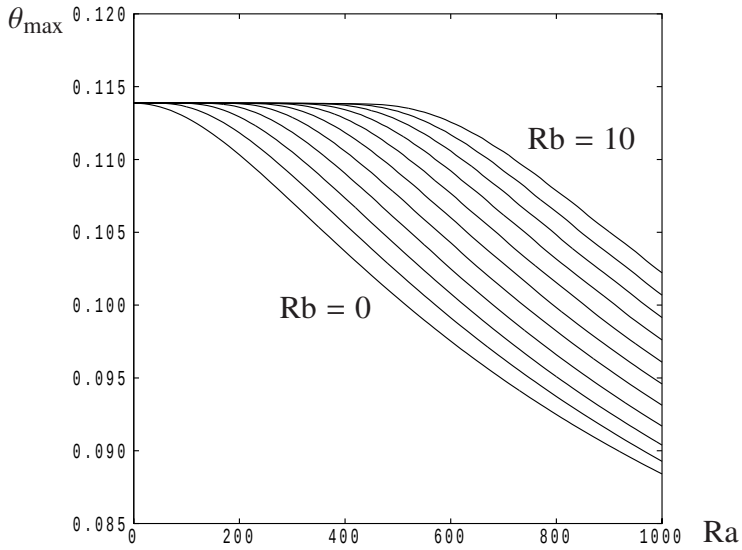

Figure 4. Variation with Ra of $\theta_{\max}$ for Rb taking integer values between 0 and 10.

Similar behaviour may be found in Figure 4 which is displays the value of $\theta_{\max}$. Here, the natural tendency is for the maximum temperature in the cavity to decrease as Ra increases. This counter-intuitive fact may be explained by the presence of a strong upflow in the middle of the cavity which brings cold fluid up from below. But here we see a straightforward monotonic variation in $\theta_{\max}$ as Ra and Rb vary. In this case the envelope of the curves has the value 0.1139, which corresponds to pure conduction.

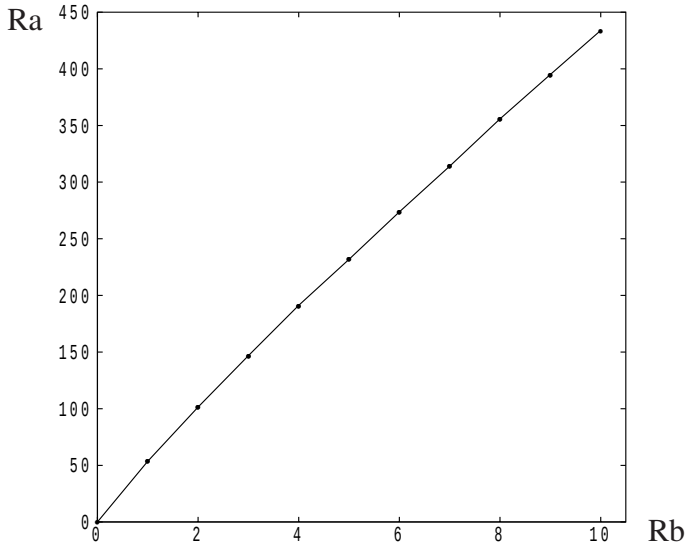

Figure 5. Variation with Rb of the critical value of Ra above which convection exists.

Although the regularisation we have used softens the threshold for flow, we may, nevertheless, attempt to evaluate the critical value of Ra at which convection begins. In the present case, we note that the Rb = 0 curve in Figure 3 rises almost perfectly linearly while $|\psi|_{\max} < 1$, and this appears to be true also for all the other curves in the range $0.5 < |\psi|_{\max} < 1$. Therefore we fitted a straight line to these separate sets of data and extrapolated to give an indication of that value of Ra for which $|\psi|_{\max} = 0$. The result of this procedure is displayed in Figure 5, where we see an almost perfectly linear variation with Rb. A rough estimate, then, is that convection ensues when

$$\mathrm{Ra} \gtrapprox 45\mathrm{Rb}. \tag{10}$$

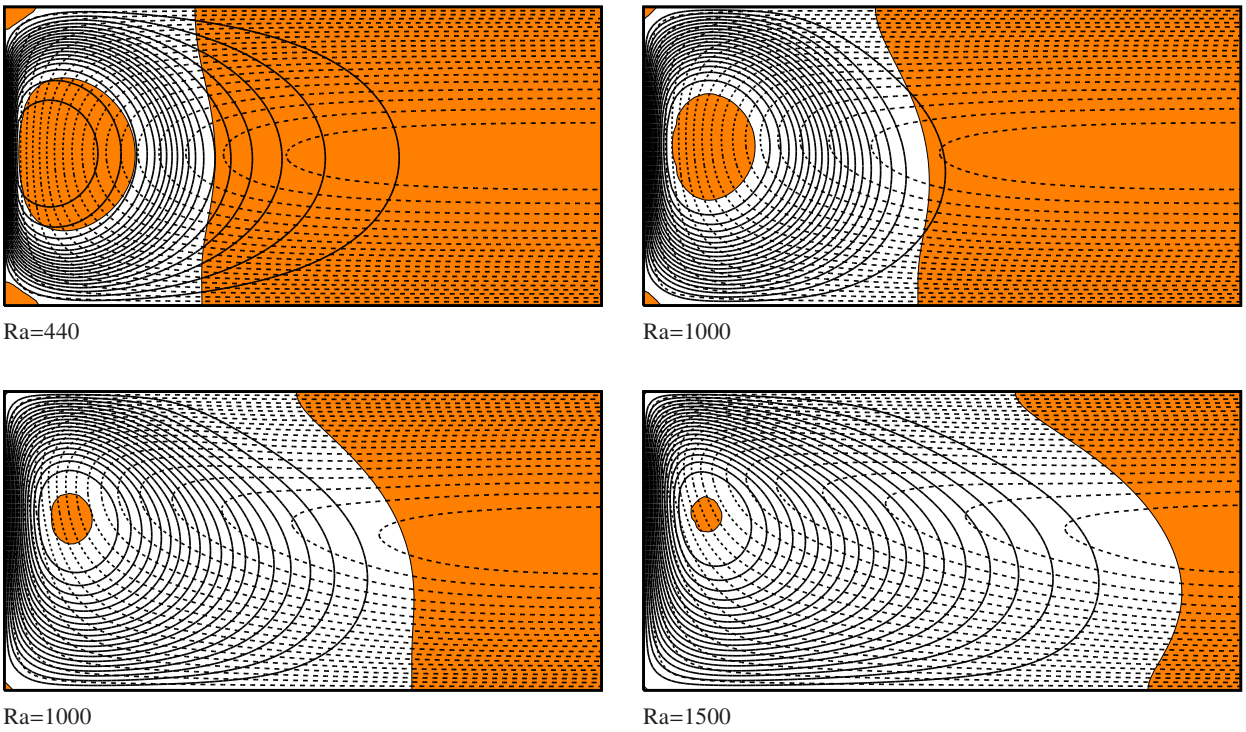

Figure 6. Streamlines (continuous) and isotherms (dashed) for $c = 100$ and Rb = 10 for a 4×1 cavity.

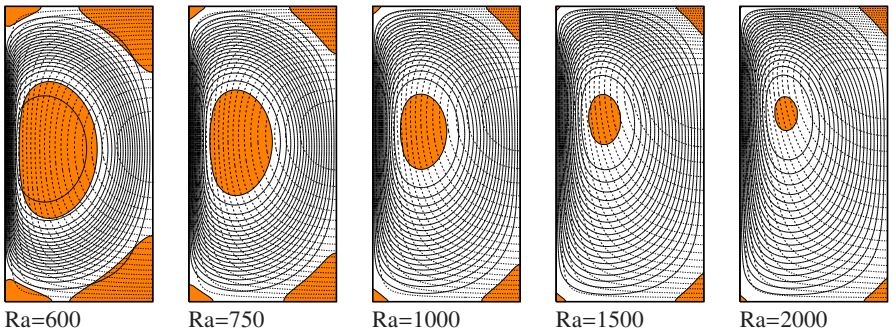

Figure 7. Streamlines (continuous) and isotherms (dashed) for $c = 100$ and Rb = 10 for a 1×1 cavity.

Finally, we conclude with a few more sample computations. Figure 6 shows how the flow and temperature fields evolve with Ra for a 4×1 cavity and Figure 7 does the same for a 1×1 cavity. In each case we use Rb = 10 and $c = 100$. At Ra = 440 in Figure 6 we see that most of the cavity has stagnant fluid, with flow taking place in approximately 25% of the cavity. Given that the isotherms are

horizontal towards the right hand side of the computational domain, then it is clear that computations with identical parameters, but in a cavity with a larger aspect ratio, will yield exactly the same flow patterns and isotherms, and will exactly the same onset criterion. Indeed, there is also a strong resemblance between this case and the appropriate one given in Figure 2. But as Ra increases we see a gradual reduction in the stagnant area, and when Ra = 1500 then 82% of the cavity admits flow.

For the 1×1 cavity shown in Figure 7, convection ensues just below Ra = 600, showing that the near-presence of the sidewalls to one another inhibits the onset of convection compared with larger aspect ratios. However, when convection does arise, it does so in a track which includes central line of symmetry of the full cavity. As Ra increases we once again see a substantial reduction in the size of the stagnant region in the centre of the circulation, and a large elevation in the location of the maximum temperature.

CONCLUSIONS

Internally-heated porous cavities always admit flow when saturated by a Newtonian fluid, but when saturated by a Bingham fluid there is a critical value of Ra above which convection arises. This critical value depends linearly on the magnitude of the Rees-Bingham number, Rb, and it expresses a balance between the magnitude of the buoyancy forces and the body force which is required to overcome the yield threshold of the fluid. Given that the largest buoyancy force occurs halfway along the vertical surfaces it is here that convection begins as Ra rises, and it is here that the fluid flow always remains the strongest. There is a gradual reduction in the size of the stagnant regions as Ra increases.

REFERENCES

Banu, N. (2000) Free convection in fluid-saturated porous media, *PhD thesis, Department of Mechanical Engineering, University of Bath, UK*.

Banu, N., Rees, D.A.S., Pop, I. (1998) Steady and unsteady convection in rectangular porous cavities with internal heat generation, *Proceedings of the 11th International Heat Transfer Conference vol. 4, pp. 375-380, Kyongju, Korea, August (1998)*.

Gasser, R.D., Kazimi, M.S. (1976) Onset of convection in a porous medium with internal heat generation, *A.S.M.E. Journal of Heat Transfer*, Vol. 98, pp. 49-54.

Nash, S., Rees, D.A.S. (2017) The effect of microstructure on models for the flow of a Bingham fluid in porous media: one-dimensional flows, To appear in: *Transport in Porous Media*.

Nouri-Borujerdi, A., Noghrehabadi, A.R., Rees, D.A.S. (2007) The onset of convection in a horizontal porous layer with uniform heat generation using a thermal non-equilibrium model, *Transport in Porous Media*, Vol. 69, pp. 343-357.

Papanastasiou, T.C. (1987) Flow of materials with yield, *Journal of Rheology*, Vol. 31, pp. 385–404.

Pascal, H. (1981) Nonsteady flow through porous media in the presence of a threshold gradient, *Acta Mechanica*, Vol. 39, pp. 207–224.

Rees, D.A.S. (2015) On convective boundary layer flows of a Bingham fluid in a porous medium, *International Journal of Heat and Mass Transfer*, Vol. 82, pp. 206-212.

Rees, D.A.S. (2016) The convection of a Bingham fluid in a differentially-heated porous cavity, *International Journal of Numerical Methods for Heat and Fluid Flow [25th Anniversary special issue]*, Vol. 26, pp. 879-896.

Rees, D.A.S., Bassom, A.P. (2015) Unsteady thermal boundary layer flows of a Bingham fluid in a porous medium, *International Journal of Heat and Mass Transfer*, Vol. 82, pp. 460-467.

Rees, D.A.S., Bassom, A.P. (2016) Unsteady thermal boundary layer flows of a Bingham fluid in a porous medium following a sudden change in surface heat flux, *International Journal of Heat and Mass Transfer*, Vol. 93, pp. 1100-1106.